Energy 69 (2014) 553–561

Contents lists available at ScienceDirect

Energy

journal homepage: www.elsevier.com/locate/energy

Numerical modeling of interconnect flow channel design and thermal stress analysis of a planar anode-supported solid oxide fuel cell stack

S.-S. Wei, T.-H. Wang, J.-S. Wu*

Department of Mechanical Engineering, National Chiao Tung University, Hsinchu, Taiwan

ARTICLE INFO

Article history:
Received 12 November 2013
Received in revised form
8 March 2014
Accepted 13 March 2014
Available online 13 April 2014

Keywords:
SOFC
CFD
thermal stress
stack
interconnect

ABSTRACT

In this paper, we propose a new design of flow channel and stack arrangement based on the numerical study considering the effect of the flow channel design on the stack performance and analyze the thermal stress of a planar anode-supported solid oxide fuel cell stack. We also attempt to simplify the cell stack design without affecting its performance and propose an easier sealing method of cell stacks through the study of the thermal stress distribution. The results indicate that the new design, created by changing the cathode flow channel to a porous current collector, with a 6.3% increase in power density, an 8.6% increase in electrical efficiency. Both more uniform flow and current density distribution can be obtained as compared with a conventional counter-flow design. In addition, we propose a new design direction of cell stack, which could be simpler and easier to fabricate, in which material can easily undertake the resulting stress based on the thermal stress analysis.

1. Introduction

A fuel cell is a device that converts chemical energy into electrical energy through an alternative, environmentally benign electro-chemical process. Compared to other renewable energy technologies, the non-renewable fuel cell is a relatively stable power generation device. In particular, fuel cell technology is gaining attention due to its high efficiency compared to combustion engines and its ability to address the depletion of natural resources and global environmental concerns by zero carbon dioxide emissions if hydrogen is used [1].

Among the different types of fuel cells, solid oxide fuel cell (SOFC) is an all-solid-state fuel cell that has been considered as one of the promising energy technologies for residential and distributed power plants due to its much higher efficiency in combination with combined heat and power (CHP), multi-fuel flexibility and potentially low production cost [2–4], even though other types of power systems have increasingly improved their efficiency over the years. Currently, there are two geometrical types of SOFCs depending on the cell structure, namely, planar and tubular. Compared to tubular cell, planar type SOFC has gained significant interest, since it can be easily produced and sealed [5]. In addition, planar SOFCs can operate at high temperatures (700–900 °C), which is particularly attractive for CHP (combined heat and power) applications, and its overall efficiency can reach up to 90% [6–8]. However, to improve the design of the SOFC–CHP system, fuel cell stacking is considered to be one of the key factors that affect the overall efficiency, in addition to the optimization of the CHP system itself.

Understanding the details of the internal processes occurring within the SOFC experimentally is an expensive and challenging procedure. Therefore, theoretical tools, such as simulation modeling, are very important in realizing the design process of an SOFC stack system. Accordingly, this study considers the detailed mass and heat transports, together with the electro-chemical reactions simultaneously, to obtain the distributions of power density, current density, fuel/oxidizer concentrations, and thermal stress, among others, under stack operation. Based on these, it is possible to optimize the stacking of fuel cells at a low cost compared to direct experiments based on a trial-and-error approach. This makes simulation as an inevitable tool in the iterative design process [9,10].

In the past, numerous numerical simulation models have been developed to predict the effects of various stack geometrical and operating parameters of SOFC. Based on these results, many designs have been reported for the planar SOFC stack, with an aim to maximize the power density and fuel utilization, and to minimize

* Corresponding author. Tel.: +886 3 573 1693; fax: +886 3 611 0023.
E-mail address: chongsin@faculty.nctu.edu.tw (J.-S. Wu).

http://dx.doi.org/10.1016/j.energy.2014.03.052
0360-5442/

the non-uniform current density distribution and temperature distribution that directly contribute to the thermal stress in different SOFC components [11–19]. Thermal stress analysis is a very important method to study systematically the performance of a system operating at high temperature, e.g., gas turbine [20], laser welding [21,22], and SOFC [23–26], to name a few, because it is generally difficult to measure the detailed properties in such harsh environment. SOFC is generally operated at high temperatures, it may have stress concentration problem, which may cause the damage of the cell stack for a long-term operation. In the past, several studies have employed the finite element method to predict the thermal stress distribution of the system which could lead to a better design of the system, which is also one of the major objectives of the current study.

For the flow channel design of a proton exchange membrane fuel cell (PEMFC), how to deal with condensed liquid water effectively is one of the critical issues. The liquid water, which is produced through chemical reactions, often easily plugs the flow channels. It results in performance deterioration of the fuel cell. In general, PEMFCs with single serpentine flow channel can easily remove liquid water by supplying enough pressure difference and also recreates a relatively uniform current density distribution (e.g., [27,28]). In contrast, the solid oxide fuel cell is operated at high temperatures. There are only gases flowing in the cell stack. Unlike the PEMFCs, the flow plates of an SOFC are used to make the temperature distribution more uniform. High-temperature gradient may lead to either fuel cell crack or failure of the sealant. Thus, the use of flow plates with parallel channels is very common in SOFC.

Recknagle et al. [29] have shown that a counter-flow channel design results in a higher power density than co-flow and cross-flow designs. However, it has been shown that the cell stack design using counter-flow channels has certain inherent disadvantages. These include non-uniform flow distribution and often very complex structures needed for coupling the fuel and air flow inlet and outlet. For efficient cell stack design, the uniform inlet flow is very important, which can decrease the temperature variation of the cell stack structure and increase the cell power density [30–32]. To circumvent these disadvantages, one may have to design a very complex geometrical configuration of inlet and outlet channels for fuel and oxidizer.

Thus, in this study we propose a new design of counter-flow channels in a cell stack for improving the uniformity of the thermal–fluid–electrical properties, based on extensive computational fluid dynamics (CFD) simulations, which not only retains the high power density characteristics but also maintains the simplicity of the design. Furthermore, we have performed the simulation of the thermal stress of the stack to verify the feasibility of the design.

Table 1
Material properties used in the benchmarked case.

Porous anode (NiO + YSZ)	Thickness	1.8 mm
	Density	6500 kg/m^3
	Specific heat	450 J/kg K
	Thermal conductivity	10 W/m K
	Electron conductivity	333,330 1/Ω-m
	Viscous resistance	1e + 13 1/m^2
	Porosity	0.24
	Tortuosity	3
	Anode transfer coeff.	0.7
	Cathode transfer coeff.	0.7
	Exchange current density	200,000
Porous cathode (LSM)	Thickness	0.03 mm
	Density	5620 kg/m^3
	Specific heat	450 J/kg K
	Thermal conductivity	11 W/m K
	Electron conductivity	7937 1/Ω-m
	Viscous resistance	1e + 13 1/m^2
	Porosity	0.375
	Tortuosity	3
	Anode transfer coeff.	0.7
	Cathode transfer coeff.	0.7
	Exchange current density	800
Electrolyte (YSZ)	Thickness	0.02 mm
	Density	5480 kg/m^3
	Specific heat	450 J/kg K
	Thermal conductivity	2 W/m K
	Resistivity	0.1
Interconnect (metal)	Density	8900
	Specific heat	446 J/kg K
	Thermal conductivity	72 W/m K
	Electron conductivity	1.5e + 07 1/Ω-m
	Anode contact resist.	1e−07 Ω-m^2
	Cathode contact resist.	1e−08 Ω-m^2

2. Numerical method

In the three-dimensional modeling work, commercial package, named ANSYS-FLUENT and ANSYS [33], which was, respectively, employed to simulate the thermal–fluid–electrical field and the thermal stress distribution within a cell stack. Initially, by using the CFD model, which includes an SOFC module, we solved the continuity, momentum, energy, and species continuity equations

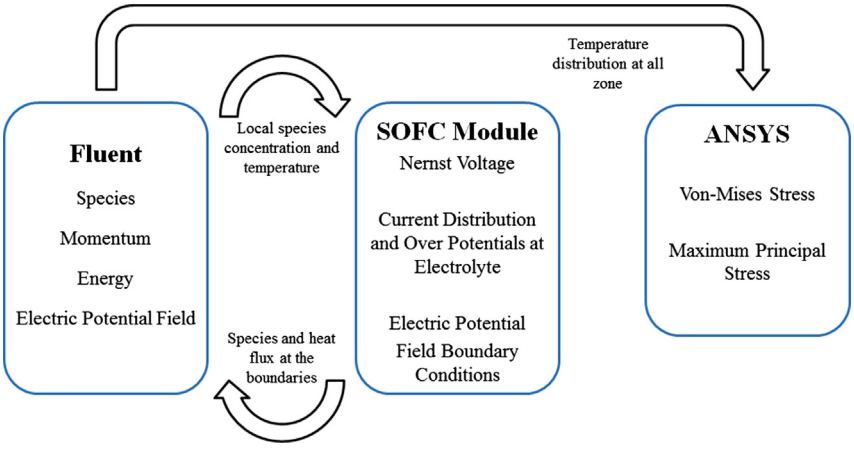

Fig. 1. Coupling of flow solver, SOFC module, and stress solver.

Table 2
Boundary conditions used in the benchmarked case.

Anode flow rate	4.48×10^{-7} kg/s
Anode flow inlet temperature	1123 K
Anode flow composition (mole %)	97%H_2, 3%H_2O
Cathode flow rate	2.17×10^{-5} kg/s
Cathode flow inlet temperature	1123 K
Cathode flow composition	100% dry air
Operating pressure	1
External boundaries	Adiabatic

coupled with the current continuity equations, and the electrochemical reactions occurring within SOFC. These equations were discretized using the finite-volume method and solved using a pressure-based algorithm in coupling velocity and pressure effectively. Following that, ANSYS, which uses the finite element method, was employed to analyze the distribution of thermal stress on a cell stack.

Fig. 1 illustrates the conceptual sketch that shows the coupling of the FLUENT flow solver and SOFC module and ANSYS stress solver. The flow solver provides the species and temperature distributions to the SOFC module, and the SOFC module returns the species and heat fluxes at the boundaries. After obtaining the temperature distribution, we used the ANSYS workbench to port the temperature distribution results of FLUENT into the ANSYS stress solver. Subsequently, we computed the stress distribution, which includes the von Mises stress in metal and the maximum principal stress in brittle (ceramic) material. Details of the description of these can be found in the user's manual of FLUENT [34] and are not described here for brevity.

The fuel cell efficiency η, is defined as follows [35]:

$$\eta = \mu_f \frac{V_c}{V_{OCV}} \times 100\%, \quad (1)$$

where μ_f is the fuel utilization coefficient, defined as the ratio of the reacted fuel to supplied fuel in the anode, V_c is the operating voltage, and V_{ocv} is the open-circuit voltage. From this definition, it is easy to realize that the electrical efficiency is proportional to the fuel utilization and operating voltage. Thus, the optimal operating conditions for the highest electrical efficiency of fuel cells may not be at the maximal power density since fuel utilization may not be the highest.

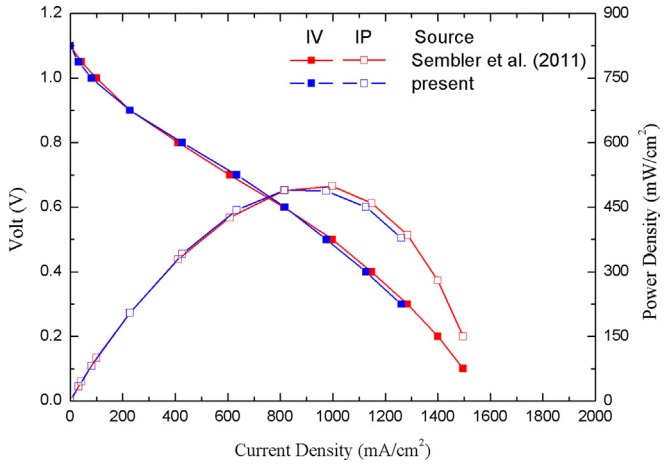

Fig. 2. Comparison of simulated *I–V* and *I–P* curves obtained with the model proposed in this study with that of Sembler and Kumar [36].

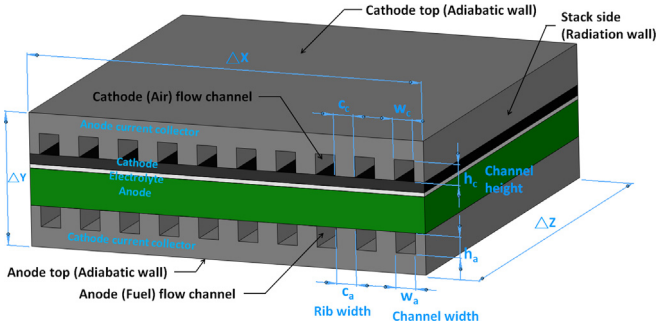

Fig. 3. External boundary conditions of Type O and nomenclature of geometric configuration of parallel counter-flow channel.

3. Results and discussion

To simplify the SOFC simulation model, the cell stack was divided into interconnect, cell, and flow channel components. Furthermore, we considered the porous electrodes as isotropic and homogeneous. Gases in the SOFC are ideal gases and heat capacities of the gaseous fluids are only functions of temperature. The fluid flow can be modeled as incompressible and laminar due to a small pressure gradient and flow channel, and flow velocities. The gas sealing is assumed to be perfect. Considering the performance, uniform distribution and convenience for fabrication, we adopted the parallel counter-flow interconnect design. Following the idea of Sembler and Kumar [36], we could estimate the performance of a cell stack by simply simulating a single cell. Thus, we simulated a single cell to improve the stack flow channel design. After the completion of flow channel design, we simulated the thermal–fluid field of a single cell with different inlet and outlet port designs, within a multi-cell stack. Finally, we simulated a three-cell stack to obtain the stress distribution of each stack component at temperatures of 700, 800, and 900 °C.

3.1. Effects of flow channel geometry on the single cell stack performance based on parallel counter-flow channel

Firstly, we benchmarked our simulation to that presented by Sembler and Kumar [36] using the same simulation conditions to ensure the validity of the SOFC model proposed in this study. The model assumes that the flow field at the channel inlet is uniform without considering the inlet and outlet port design. Tables 1 and 2 summarize the material properties and boundary conditions, respectively, employed in the simulation model discussed in this study. Here, the anode, cathode, and electrolyte are made of NiO + YSZ, LSM, and YSZ, respectively. The H/O (molar) ratio is kept as 1.11 throughout the study, unless otherwise specified. For the benchmarking case, we have set up the grid size following Sembler and Kumar [36] and we have performed a thorough grid convergence test (~100 K, ~200 K, and ~400 K cells) and finally decided

Table 3
Power density with various geometric configurations of the flow channels at 0.6 V.

Type	Configurations (mm)						Power density (mW/cm²)	Electrical efficiency
	h_a	h_c	w_a	w_c	c_a	c_c		
A	1	1	1	1	1	1	752.2	49.2%
B	0.5	1	1	1	1	1	758.5 (0.83%)	49.6%
C	1	0.5	1	1	1	1	754.9 (0.36%)	49.6%
D	1	1	2	1	1	1	755.5 (0.44%)	49.3%
E	1	1	1	2	1	1	753.1 (0.12%)	49.7%
F	1	1	1.4	1.4	0.6	0.6	767.4 (2%)	50.7%

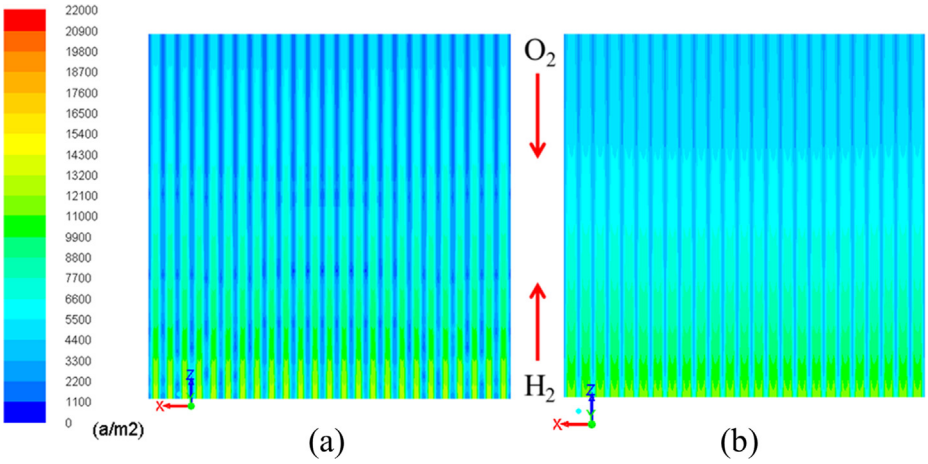

Fig. 4. Comparison of the current density distributions of (a) Type A, (b) Type F.

to use about 200 K cells for the results presented next because the results of 200 K cell are almost the same as those of 400 K cells. Fig. 2 shows that the simulated *I–V* and *I–P* curves are in excellent agreement with those obtained by Sembler and Kumar [36]. The results clearly validate the current SOFC model.

Secondly, we performed a parametric study of the flow channel configuration for optimizing power generation. Fig. 3 illustrates the geometrical configuration of the planar parallel counter-flow design. Important parameters include the widths of anode and cathode flow channels (w_a, w_c), the height of anode cathode flow channel (h_a, h_c) and the width of current collector (interconnect) contact with the cell (c_a, c_c). In the configurations considered in this study, the cell dimension is fixed as 50 mm × 50 mm with different combinations of c_a, c_c, w_a, w_c, h_a, and h_c. Furthermore, to make the simulation results more close to our experiment currently in progress, we changed the anode thickness to 1 mm and the cathode thickness to 0.1 mm. In addition, the external boundaries were set as adiabatic at the top of the stack and radiation walls at the sides of the stack at 1123 K, as shown in Fig. 3. Other parameters and conditions are the same as those listed in Tables 1 and 2. Note that the electrolyte between the anode and cathode is intentionally enlarged in the sketch for a clear view.

Table 3 summarizes the power density and electrical efficiency at 0.6 V with various geometrical configurations of the flow channels (Types A–F). It shows that the electrical efficiency of Type A is 49.2%. In addition, the results indicate that the changes in power density and electrical efficiency due to variation of flow channel sizes were relatively small. However, the current density distribution became more uniform when the contact area between the cell and the current collector of cathode becomes smaller (Fig. 4a, b). Because of the anode-supported structure, the cathode is comparatively thin (20–100 μm). As the rib width of the current collector at the cathode side become smaller, the channel width for flowing air becomes larger. This results in that it becomes easier for the air (especially oxygen) to diffuse into the cathode region which is located near the rib. In addition, if the rib width is larger, the diffusion of the oxygen into the cathode region near the rib will cause a large drop of the oxygen concentration because of electrochemical reactions. Therefore, the contact area of the cathode current collector with the cathode has a remarkable effect on oxygen distribution and of course overall cell performance. However, it is not easy to fabricate very thin straight-rib interconnects and there may also be a problem related to structural strength under high-temperature environment. Ideally, the current collector at the cathode side of the anode-support solid oxide fuel cell should have a uniform contact with the cathode, but with a minimal contact area. This observation leads us to replace the straight-rib type flow channel design with the porous current collector at the position between the cathode and the interconnect. The porous media current collector design is relatively easy to fabricate using electric porous cermet or metal mesh, as shown in Fig. 5. In addition, we would expect the cell has a better stress distribution since the contact is more uniformly distributed.

For this reason, we changed the cathode current collector of the parallel flow channel to a porous media with a height of 1 mm and a porosity of 0.6 in the simulation, which we denote as Type G. Fig. 6 compares the simulated *I–V* and *I–P* curves of Type A and Type G. Results indicated that the maximal power density, fuel utilization,

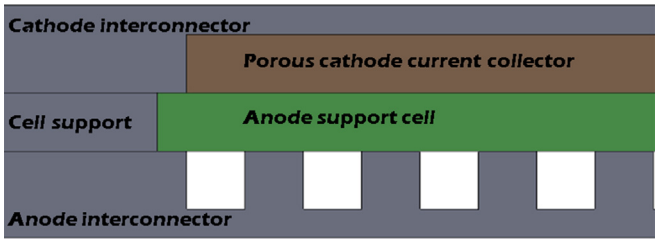

Fig. 5. The geometrical diagram of a porous cathode current collector, terms as Type G.

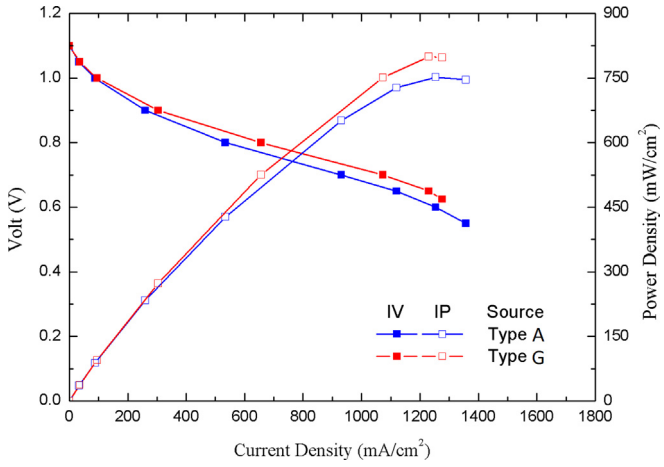

Fig. 6. Comparison of *I–V* and *I–P* curves of Type A and Type G.

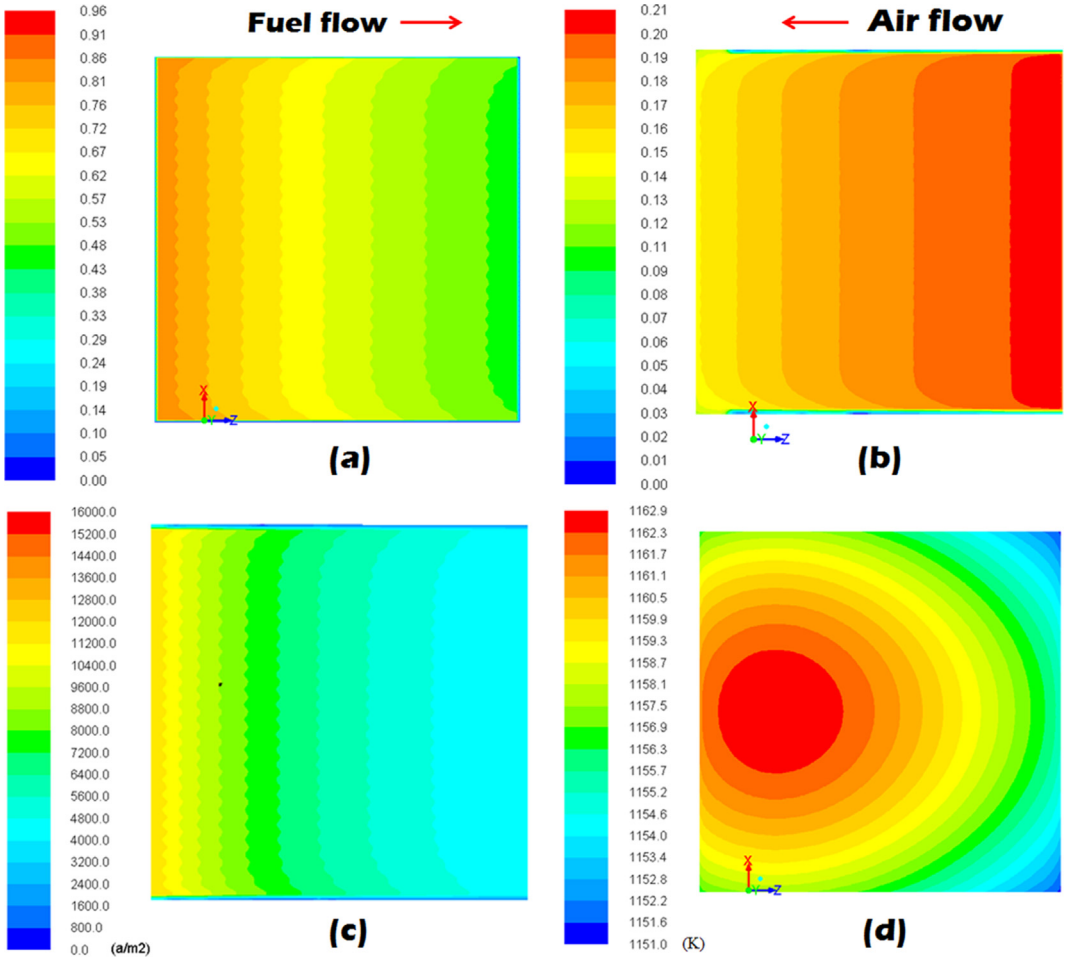

Fig. 7. Typical distribution of properties with porous media cathode current collector (Type G) with 0.8 V: (a) fuel mole fraction, (b) O_2 mole fraction, (c) current density, and (d) temperature.

and electrical efficiency with a porous media cathode current collector increase 6.9%, 8.6%, and 8.6%, respectively, as compared to that of Type A. Fig. 7 shows some typical distribution of the properties with a porous media cathode current collector when the voltage is 0.8 V. In practice, either a corrugated interconnect, which can be easily fabricated [24], or metal mesh [15] can be used as the equivalent porous media at the cathode interconnect, to reduce the contact area between cathode and the interconnect.

We think the uniform flow can have greatest temperature distribution and power efficiency. In general, we need the design in the front of cell flow channel to build uniform inlet flow; because of our design is counter-flow channel, the inlet flow and outlet flow tube at the same side. This design we will continue to discuss in the following.

3.2. Stack design

For cell stack design, especially on the fuel flow side, a uniform inlet flow is very important. Fig. 8 shows the proposed design of a

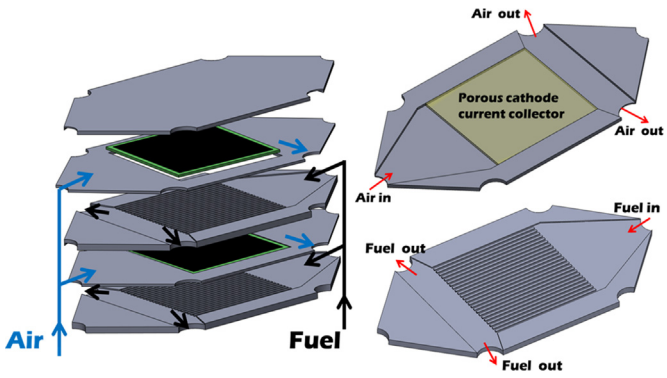

Fig. 8. Sketch of hexagonal cell stack design (denoted as Type H).

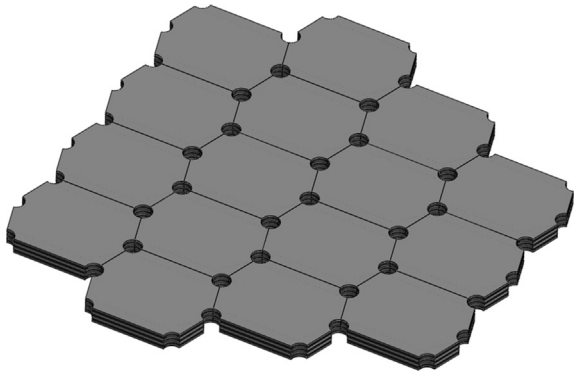

Fig. 9. Sketch of multi-cell multi-stack arrangement.

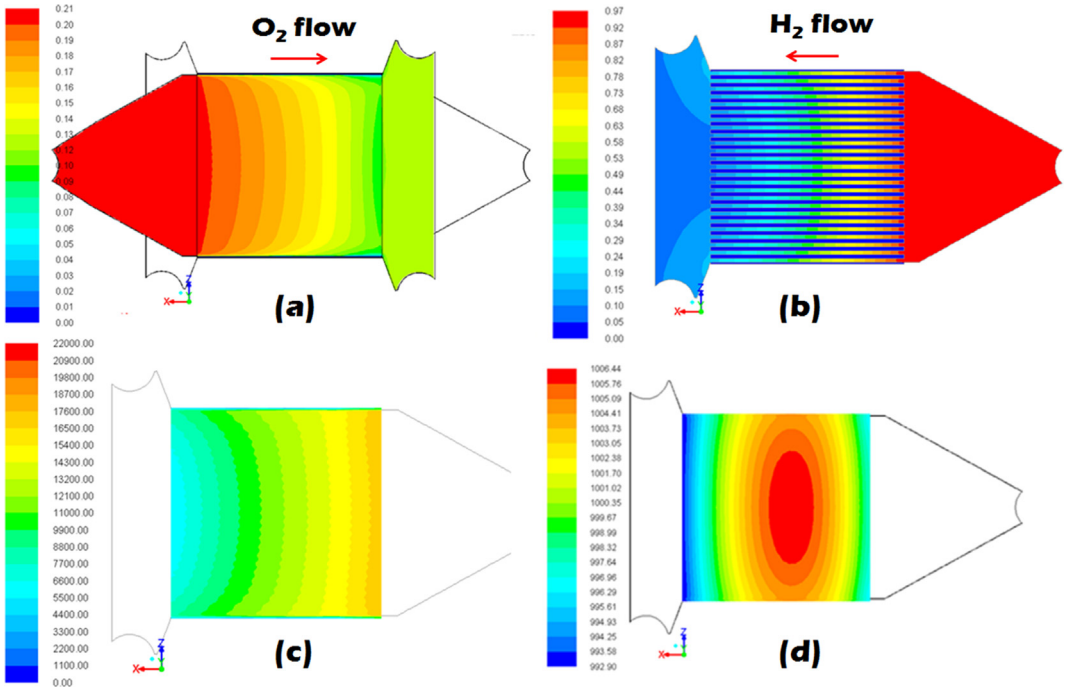

Fig. 10. Distribution of properties with H/O ratio = 1.11 and 0.65 V (a) O_2 mole fraction, (b) H_2 mole fraction, (c) current density distribution, and (d) temperature distribution.

multi-cell stack. It is a hexagonal cell stack consisting of planar anode-supported SOFCs of area 50 × 50 mm^2, with a single-inlet and a double-outlet design for both the anode and cathode, based on a Type G arrangement (Fig. 5). The air and fuel flow in opposite directions (counter flow). If we include more stacks, it looks like a honeycomb structure (Fig. 9). Each flow pipe is shared by three stacks. This design has the potential to reduce the problem of using a large-scale cell and multi-stack system, termed as Type H.

Since we are interested in developing an SOFC system running at intermediate temperature, we have changed the inlet temperature radiation wall to 973 K and heat transfer coefficient to 0.5. Fig. 10 shows the typical simulated distribution of single planar SOFC properties in a Type H stack with an H/O ratio of 1.11 and a voltage of 0.65 V. We can see that, with the simple design of a single inlet and two outlets, inflow distribution is fairly uniform, similar to that in Type G, even though H_2 concentrations are slightly higher at the sides than those in the middle. To further improve this situation, we can simply change the inlet flow diffusion channel to be more "constricted" to make the inlet flow more uniform (Fig. 11), which is clearly demonstrated in Fig. 12. This is much simpler than adding flow deflectors at the diffusion side by xHuang et al. [30].

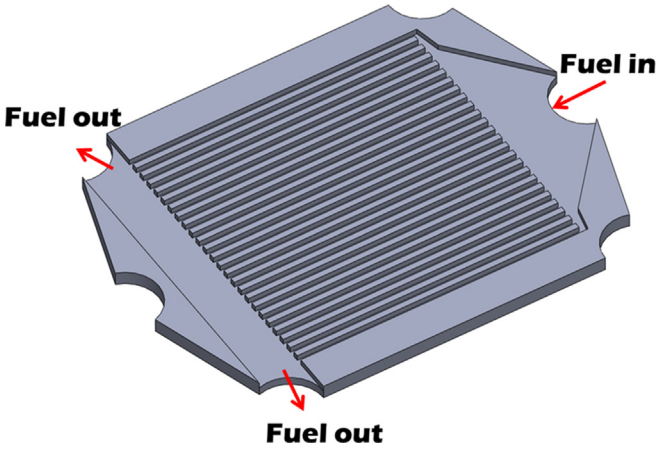

Fig. 11. Sketch of hexagonal cell stack new design, termed as Type H new.

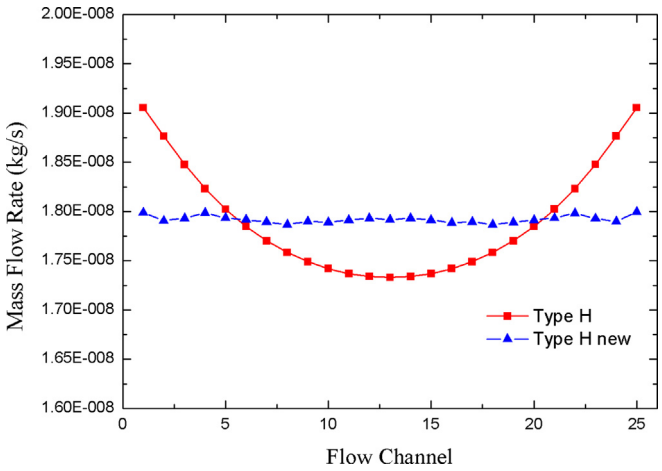

Fig. 12. Distribution of mass flow rate of anode flow side with Type H and Type H new.

Table 4
Mechanical properties of metal material used in the simulations [37,38].

Properties	Interconnect (structure steel)	Steel wire mesh
Density (kg/m^3)	7850	3680
CTE (Reference T)	1.2 × 10^{-5}/°C (22 °C)	1.2 × 10^{-5}/°C (22 °C)
Young's modulus (GPa)	200	140
Poisson's ratio	0.3	0.3
Bulk modulus (GPa)	166.6	116.6
Shear modulus (GPa)	76.9	53.8

CTE, coefficient of thermal expansion.

Table 5
Mechanical properties of brittle material [39–44].

Properties	Ni + YSZ (40:60) porosity 40%	LSM porosity 30%	Grancrete
Density (kg/m^3)	6500	5620	2000
CTE (Reference T)	1.25 × 10^{-5}/°C (700 °C)	1.05 × 10^{-5}/°C (700 °C)	1 × 10^{-6}/°C (20 °C)
Young's modulus (GPa)	50	47.5	4.14
Poisson's ratio	0.387	0.3	0.2
Bulk modulus (GPa)	73.75	39.6	2.3
Shear modulus (GPa)	18	18.3	1.725

3.3. Stress distribution of 3-cell stack

Sealing material is a very important factor in the current cell stack practice. It prevents leakage of gas and decreases cell damage caused by the cell stack in the course of thermal expansion [37]. Due to the design of the cell stack, which requires a cell support to maintain the airtightness between the air and fuel flow channel, the use of the sealing process becomes very cumbersome. Therefore, we consider direct use of sealing materials for the support frame to reduce the complexity of the cell stack. The material used is ceramics or others. In this case, we use the Grancrete [38] which has a better strength (maximum strength is about 41 Mpa) and higher resistance to high temperature related cracking. In addition, it can be easily molded into various shapes, which eventually reduces the cell stack manufacturing cost.

With this aim in mind, we analyzed the stress distribution of a three-cell stack of Type H using ANSYS software. Tables 4 and 5 summarize the mechanical properties of "metal" and "brittle" materials, respectively [39–46]. In general, the cell stack damage is usually located in brittle materials. By analyzing the stress distribution and maximum principal stress, it is possible to understand whether the current design can withstand the operating conditions we are interested in. Similarly, we have performed a thorough grid convergence test and we have decided to employ ~1.6 million elements for the CFD simulation and about 0.3 million elements for the stress simulation in the 3-cell stack design for all the results presented next.

Figs. 13 and 14 shows the maximal principal stress distribution for the anode and the cathode at 970 K, respectively, which uses different types of cell support materials. The results show that the use of Grancrete cell support can effectively reduce the maximum principal stress of the cell, which the failure is defined by the maximum principal stress exceeds the ultimate tensile strength of the brittle materials. Note the maximum material strength of the anode-supported cell (NiO-YSZ-LSM) is about 187 Mpa (RT) ~ 112 Mpa (800 °C) [47]. Instead, the cathode could be damaged, should the

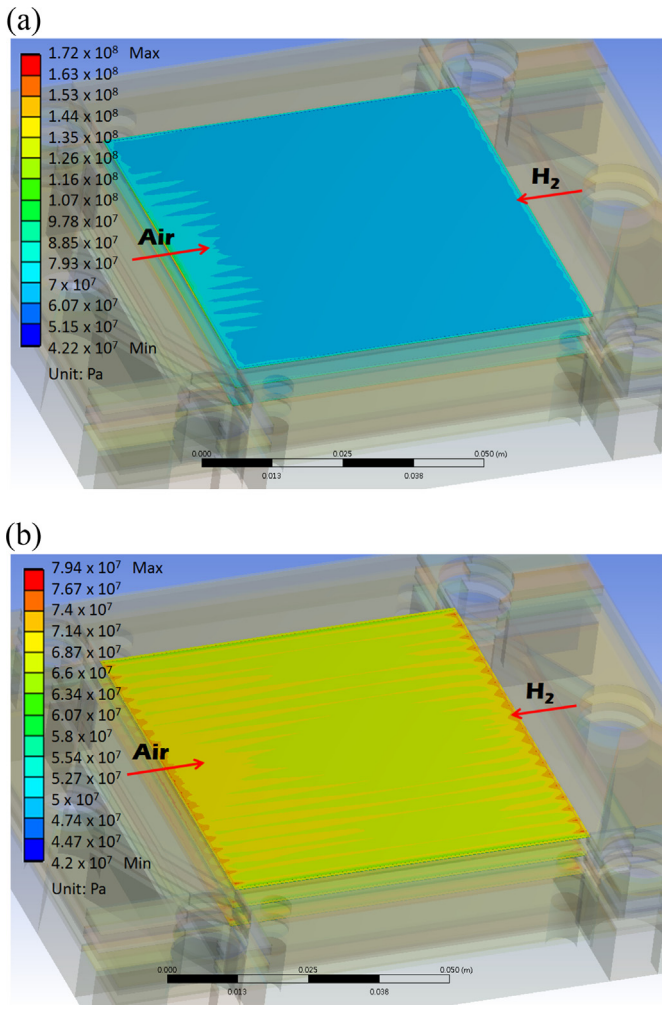

Fig. 13. Distribution of maximum principal stress of anode at 2.4 V, 970 K (a) max: 77.4 Mpa using steel cell support and (b) max: 57.1 Mpa using Grancrete cell support. Maximum principal stress of cathode: 112 Mpa (800 °C).

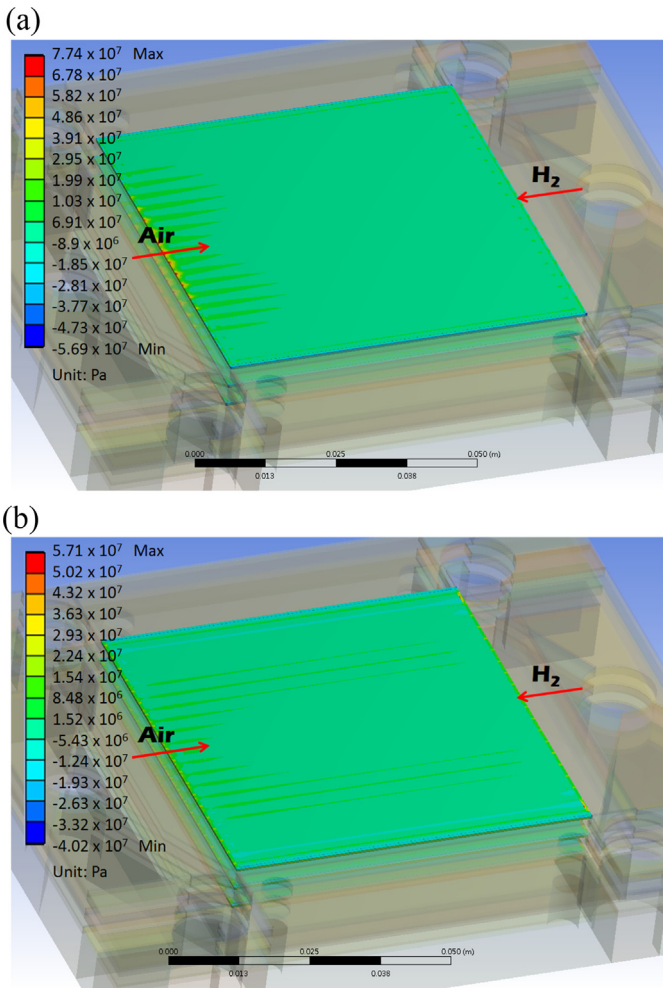

Fig. 14. Distribution of maximum principal stress of cathode at 2.4 V, 970 K (a) max: 172 Mpa using steel cell support and (b) max: 79.4 Mpa using Grancrete cell support. Maximum principal stress of cathode: 112 Mpa (800 °C).

steel support be used (Fig. 14a). Therefore, it is better to use other sealing materials or sealing designs in the steel cell support.

Fig. 15 shows the distribution of von Mises stress of steel cell support and maximum principal stress of Grancrete cell support at 970 K, respectively. It can be seen that stainless steel cell support and Grancrete cell support can both withstand the thermal stress under the specified operation of the cell. In Fig. 15a, the simulated maximum von Mises stress is 342 Mpa, which is slightly lower than the yield strength of stainless steel 430 (363 Mpa). However, the cathode is already damaged under this operating condition, as shown in Fig. 14a. In addition, the stress is more concentrated near the air inlet flow diffusion side of the cell support, which is mainly caused by the large temperature gradient and large thermal expansion coefficient of the stainless steel at this location. In Fig. 15b, the simulated maximal principal stress is 21.7 MPa that is much smaller than the maximal principal stress of the Grancrete material (41 MPa). The stress is also concentrated near the inlet flow diffusion side of the cell support due to the large temperature gradient, but it is far below the material strength because of very low thermal expansion coefficient.

Fig. 16 shows the maximum principal stress of anode-supported cell cathode and Grancrete cell support at the operating temperatures from 700 °C to 900 °C by using Grancrete cell support. We can see even if the operating temperature is raised up to 900 °C, the current stack design using Grancrete cell support is still very safe considering the maximal principal stress is still well below the material strength.

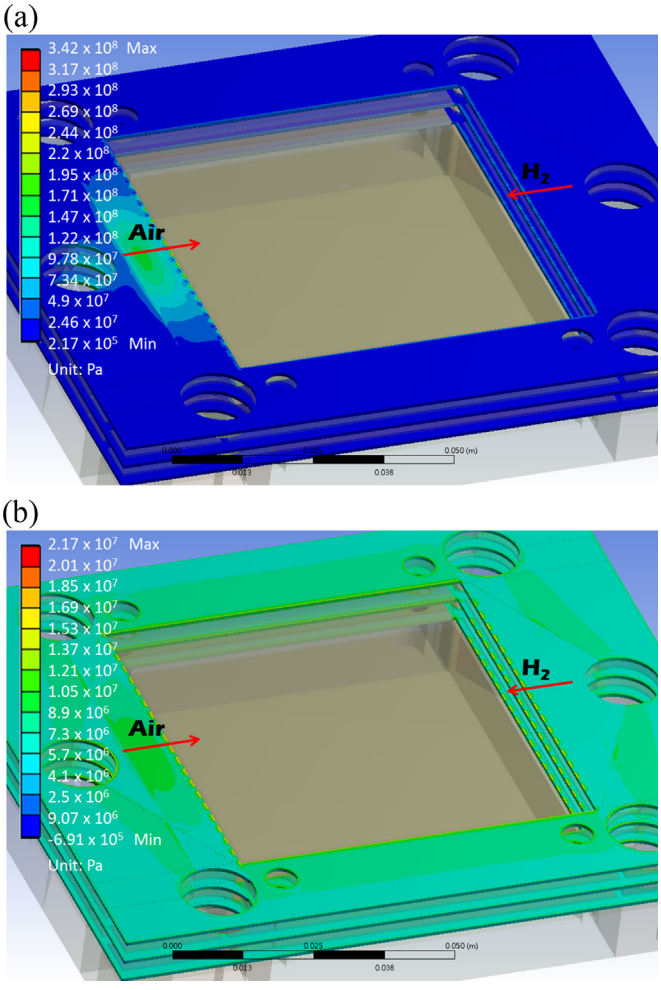

Fig. 15. Distribution of (a) von Mises stress of steel cell support, max: 342 Mpa (b) maximum principal stress of Grancrete, max: 21.7 Mpa, at 2.4 V, 970 K.

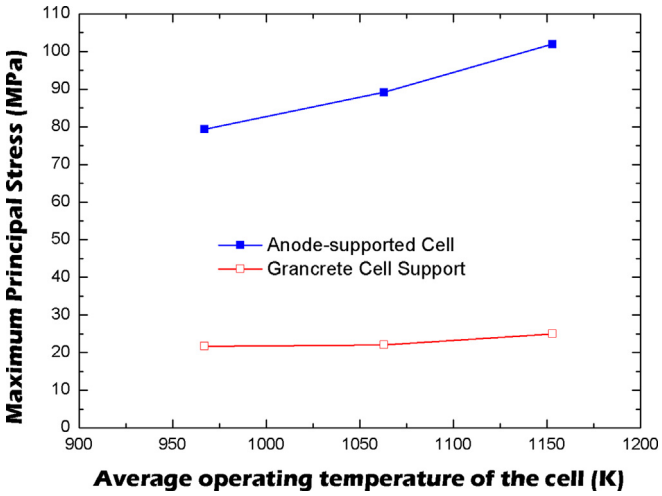

Fig. 16. Maximum principal stress of anode-supported cell using Grancrete cell support, 970–1160 K. Maximum strength of cell: 187 Mpa (RT)–112 Mpa (800 °C); maximum strength of Grancrete: about 41 Mpa.

4. Conclusion

In the current study, effects of the geometry of flow channels of interconnect, inlet and outlet port designs, and stress distribution of the design, have been numerically investigated for a counter-flow planar anode-supported SOFC (50 × 50 mm^2) stack. The major findings are summarized as follows:

1. Use of a porous media current collector at the cathode side increases the maximal power density, fuel utilization, and electrical efficiency by 6.9%, 8.6%, and 8.6%, respectively. Uniformity of the flow across the channels can be greatly improved by a constricted inlet flow port design as proposed in the current study.
2. The stack design proposed in this study has the potential in producing more uniform flow and current density distribution.
3. Lower stress distribution using cheaper materials, e.g., Grancrete for the cell support, could be achieved based on the thermal stress analysis.

Corresponding experiments on validating the simulations are currently in progress and will be reported in the very near future.

Acknowledgments

The financial support provided by the National Science Council of Taiwan through Grants no. NSC-99-3113-P-009-005, NSC-101-3113-P-009-002 and NSC-102-3113-P-009-001 is highly appreciated.

References

[1] Steele BCH, Heinzel A. Materials for fuel-cell technologies. Nature 2001;414:345–52.
[2] Tao SW, Irvine JTS. A redox-stable efficient anode for solid-oxide fuel cells. Nat Mater 2003;2:320–3.
[3] Singhal SC. Solid oxide fuel cells for stationary, mobile and military applications. Solid State Ion 2002;152–153:405–10.
[4] Park S, Vohs JM, Gorte RJ. Direct oxidation of hydrocarbons in a solid-oxide fuel cell. Nature 2000;404:265–7.

[5] Penner SS, Appleby AJ, Baker BS, Bates JL, Buss LB, Dollard WJ, et al. Commercialization of fuel cell. Energy 1995;20:331–470.
[6] Liso Vincenzo, Olesen Anders Christian, Nielsen Mads Pagh, Kær Søren Knudsen. Performance comparison between partial oxidation and methane steam reforming processes for solid oxide fuel cell (SOFC) micro combined heat and power (CHP) system. Energy 2011;36:4216–26.
[7] Wu DW, Wang RZ. Combined cooling, heating and power: a review. Science 2006;32:459–95.
[8] Colella WG. Modelling results for the thermal management sub-system of a combined heat and power (CHP) fuel cell system (FCS). J Power Sources 2003;118:129–49.
[9] Singhal SC, Kendall K, editors. High temperature solid oxide fuel cells: fundamentals, design and applications. 1st ed. Oxford, UK: Elsevier Ltd.; 2003.
[10] Fuel cell handbook. 7th ed. U.S. DOE, National Energy Technology Laboratory; November 2004.
[11] Yakabe H, Baba Y, Sakurai T, Satoh M, Hirosawa I, Yoda Y. Evaluation of residual stresses in a SOFC stack. J Power Sources 2004;131:278–84.
[12] Weil KS, Koeppel BJ. Comparative finite element analysis of the stress-strain states in three different bonded solid oxide fuel cell seal designs. J Power Sources 2008;180:343–53.
[13] Chiang LK, Liu HC, Shiu YH, Lee CH, Lee RY. Thermo-electrochemical and thermal stress analysis for an anode-supported SOFC cell. Renew Energy 2008;33:2580–8.
[14] Haltiner KJ, Mukerjee S. US Patent No. 2007/0248867 A1; 2005.
[15] Anil Vasudeo Virkar, Prouse DW, Smith PC, Guang-Young Lin. US Patent No. 6770395 B2; 2004.
[16] Nguyen QM, Craig RH, US Patent No. 5290642; 1994.
[17] Chen Qiuyang, Wang Qiuwang, Zhang Jian, Yuan Jinliang. Effect of bi-layer interconnector design on mass transfer performance in porous anode of solid oxide fuel cells. Int J Heat Mass Transf 2011;54:1994–2003.
[18] Qu Zuopeng, Aravind PV, Boksteen SZ, Dekker NJJ, Janssen AHH, Woudstra N, et al. Three-dimensional computational fluid dynamics modeling of anode-supported planar SOFC. Int J Hydrogen Energy 2011;36:10209–20.
[19] Bedogni S, Campanari S, Iora P, Montelatici L, Silva P. Experimental analysis and modeling for a circular-planar type IT-SOFC. J Power Sources 2007;171(2):617–25.
[20] Mustafa AH, Hashmi MS, Yilbas BS, Sunar M. Investigation into thermal stresses in gas turbine transition-piece: Influence of material properties on stress levels. J Mater Process Technol 2008;201:369–73.
[21] Olabi AG, Benyounis KY, Hashmi MSJ. Application of response surface methodology in describing the residual stress distribution in CO_2 laser welding of AISI304. Strain 2007;43:37–46.
[22] Anawa EM, Olabi AG. Control of welding residual stress for dissimilar laser welded materials. J Mater Process Technol 2008;204:22–33.
[23] Faes A, Frandsen HL, Kaiser A, Pihlatie M. Strength of anode-supported solid oxide fuel cell. Fuel Cells 2011;11(5):682–9.
[24] An K. Mechanical properties and electrochemical durability of solid oxide fuel cell; 2003 [Advisory committee: Reifsnider KL, Prather CL, Hendricks SL, Lesko JJ, Case SW].
[25] Jingjing Tong, Xiaojia Du, Minfang Han. The development of sealant for planar SOFC. ECS Trans 2013;57(1):2395–401.
[26] Mahapatra MK, Lu K. Glass-based seals for solid oxide fuel and electrolyzer cells – a review. Mater Sci Eng 2010;67:65–85.
[27] Carton JG, Olabi AG. Design of experiment study of the parameters that affect performance of three flow plate configurations of a proton exchange membrane fuel cell. Energy 2010;35:2796–806.
[28] Carton JG, Lawlor V, Olabi AG, Hochenauer C, Zauner G. Water droplet accumulation and motion in PEM (proton exchange membrane) fuel cell mini-channels. Energy 2012;39:63–73.
[29] Recknagle KP, Williford RE, Chick LA, Rector DR, Khaleel MA. Three-dimensional thermo-fluid electrochemical modeling of planar SOFC satcks. J Power Sources 2003;113:109.
[30] Huang CM, Shy SS, Lee CH. On flow uniformity in various interconnects and its influence to cell performance of planar SOFC. J Power Sources 2008;183:205–13.
[31] Huang CM, Shy SS, Li HH, Lee CH. The impact of flow distributors on the performance of planar solid oxide fuel cell. J Power Sources 2010;195:6280–6.
[32] Yuan Ping, Liu Syu-Fang. Numerical analysis of temperature and current density distribution of a planar solid oxide fuel cell unit with nonuniform inlet flow. Numer Heat Transf Part A: Appl 2007;51(10):941–57.
[33] ANSYS Web site. Available from: http://www.ansys.com.
[34] Ansys 13.0 user's manual.
[35] Larminie James, Dicks Andrew. In: Fuel cell systems explained. 2nd ed. John Wiley & Sons; 2003. pp. 25–44.
[36] Sembler William J, Kumar Sunil. Modification of results from computational-fluid-dynamics simulations of single-cell solid-oxide fuel cells to estimate multicell stack performance. J Fuel Cell Sci Technol 2011;8.
[37] Weil KS, Koeppel BJ. Thermal stress analysis of the planar SOFC bonded compliant seal design. Int J Hydrogen Energy 2008;33:3976–90.
[38] Grancrete Web site. Available from: http://www.grancrete.net/.
[39] ANSYS engineering date sources.
[40] Gambhir ML. Concr Technol 2004;3e:390–1.
[41] Pihlatie Mikko, Kaiser Andreas, Mogensen Mogens. Mechanical properties of NiO/Ni–YSZ composites depending on temperature, porosity and redox cycling. J Eur Ceram Soc 2009;29:1657–64.
[42] Radovic M, Lara-Curzio E, Trejo RM, Wang H, Porter WD. Thermophysical properties of YSZand Ni-YSZ as a function of temperature and porosity. Adv Solid Oxide Fuel Cells II; 2007:79–85.
[43] Giraud Sophie, Canel Jérôme. Young's modulus of some SOFCs materials as a function of temperature. J Eur Ceram Soc 2008;28:77–83.
[44] Johnson Janine, Qu Jianmin. Effective modulus and coefficient of thermal expansion of Ni–YSZ porous cermets. J Power Sources 2008;181:85–92.
[45] Vaidya Sushrut, Kim Jeong-Ho. Continuum mechanics of solid oxide fuel cells using three-dimensional reconstructed microstructures. Continuum Mech – Prog Fundam Eng Appl; 2012:73–88.
[46] Virkar AV. SOFC materials and processing issues, presented at the SECA core technology program workshop; 2001.
[47] Lin Chih-Kuang, Chen Tsung-Ting, Chyou Yau-Pin, Chiang Lieh-Kwang. Thermal stress analysis of a planar SOFC stack. J Power Sources 2007;164:238–51.